Substrate-induced reduction of graphene thermal conductivity

S. V. Koniakhin,[1,2,*] O. I. Utesov,[3,†] I. N. Terterov,[1] and A. V. Nalitov[4]
[1]*St. Petersburg Academic University, Khlopina 8/3, 194021 St. Petersburg, Russia*
[2]*Ioffe Physical-Technical Institute of the Russian Academy of Sciences, 194021 St. Petersburg, Russia*
[3]*Petersburg Nuclear Physics Institute NRC "Kurchatov Institute," Gatchina, St. Petersburg 188300, Russia*
[4]*School of Physics and Astronomy, University of Southampton, Southampton SO17 1BJ, United Kingdom*
(Received 2 September 2016; revised manuscript received 23 November 2016; published 23 January 2017)

We develop a theory of heat conductivity in supported graphene, accounting for coherent phonon scattering on disorder induced by an amorphous substrate. We derive spectra for in-plane and out-of-plane phonons in the framework of Green's function approach. The energy parameters of the theory are obtained using molecular dynamics simulations for graphene on a SiO_2 substrate. The heat conductivity is calculated by the Boltzmann transport equation. We find that the interaction with the substrate drastically reduces the phonon lifetime and completely suppresses the contribution of flexural (ZA) phonons to the heat conductivity. As a result, the total heat conductivity is reduced by several times, which matches with the tendency observed in the available experimental data. The considered effect is important for managing the thermal properties of graphene-based electronic devices.

DOI: 10.1103/PhysRevB.95.045418

I. INTRODUCTION

Due to its outstanding properties, graphene, a honeycomb monolayer of carbon atoms, attracts great attention as a material for application in future nanoscale electronics. The mechanical [1,2] and electronic [3–5] properties of graphene, and the various radiation driven effects [6–8] and thermoelectric [9] phenomena in graphene are among the hottest topics of recent studies in condensed matter physics.

Along with other carbon-based materials, graphene reveals extremely high thermal conductivity κ. The room-temperature thermal conductivity of suspended graphene reaches 5000 $W\,m^{-1}\,K^{-1}$ [10–13]. For application of graphene as a component of electronic devices and for controlling the carrier density, it is commonly gated. This requires close contact between a graphene sheet and a dielectric substrate like SiO_2.

Electron scattering on the surface charged impurities [5,14], surface corrugations [15–17], atomic steps [18], and surface polar phonons [19–21] reduces the electric conductivity of graphene. The same effect is expected for the heat conductivity. Accounting for graphene layers and conductive traces as heat sinks requires a quantitative estimate of this effect. Also, estimations of acoustic phonon lifetimes and the mean free path are mandatory for calculating the phonon drag contribution to the thermopower in graphene [22,23].

Previously, the effect of the substrate on the thermal properties of graphene was investigated experimentally, from a theoretical standpoint, and by molecular dynamics simulations. The experimental studies of heat conductivity in suspended graphene are based on the Raman optothermal method [24–29], and reveal values above 2000 $W\,m^{-1}\,K^{-1}$. The investigation of supported graphene thermal properties is based on electrical heating and gives several times lower values of the thermal conductivity [30]. Other works, where supported graphene is studied, focus mainly on the electrical properties of graphene with the heat conductivity being a secondary result [31,32]. The table in Ref. [11] summarizes current studies on graphene thermal conductivity.

The heat conductivity is governed by the phonon dispersion and relaxation processes [10,11]. The theoretically investigated mechanisms of phonon relaxation include boundary scattering, point defect scattering, and anharmonic processes [33–36]. The effect of the substrate is out of consideration in most current theoretical works. In the supplementary online materials of Ref. [30], the spot contact model within the Fermi golden rule formalism developing the Klemens approach [37] for phonon scattering, was employed to account for a substrate. However, the case of randomly distributed defects with close to atomic concentration needs a theory based on Green's functions to account for coherent scattering.

Molecular dynamics (MD) is also used to investigate the thermal conductivity of graphene [38–41] and carbon nanotubes [42,43]. Such studies include modeling of the phonons of graphene on amorphous substrates. Reference [44] is devoted to molecular dynamics simulations of graphene on a SiO_2 substrate and shows that van der Waals interactions reduce the relaxation time of intrinsic acoustic phonons in graphene. The nonequilibrium MD simulation demonstrates a reduction of the thermal transport in graphene on SiO_2 [45]. Although MD simulations are a promising and powerful tool for investigating vibrational properties of solids, it is necessary to compare the obtained results with independent analytical approaches.

Here, we address the effect of an amorphous substrate on the phonon dispersion and lifetimes in graphene within the Green's function formalism [46]. The parameters of the perturbing substrate-induced van der Waals potential required by the developed analytical theory were obtained with MD simulations. In-plane (LA,TA) and flexural (ZA) phonons were considered and the corresponding contributions to heat conductivity were obtained within the Boltzmann transport equation (BTE) approach. The optical phonons were not considered due to their small occupation number at actual temperatures, which results in low contribution to thermal conductivity (see Refs. [47,48]).

*kon@mail.ioffe.ru
†utiosov@gmail.com

The rest of the paper is organized as follows. In the beginning of Sec. II A, we introduce the general form of the graphene Hamiltonian accounting for interaction with the substrate. In Secs. II B and II C, we derive spectra for the in-plane (Sec. II B) and flexural (Sec. II C) phonons within the perturbation theory approach. In Sec. II D, we describe the MD simulation, performed to estimate the energy parameters, required by the developed perturbation theory. Section III aggregates the results for spectra, phonon lifetimes, and heat conductivity. In Sec. III A, we justify the localization of ZA phonons. In Sec. III B, we discuss the mechanisms of phonon damping in graphene. The lifetime estimations for in-plane phonons are given in Sec. III C and the results for supported graphene heat conductivity are presented and discussed in Sec. III D.

II. THEORY

A. Perturbations to conventional graphene Hamiltonian due to the substrate

We start with considering the static properties of graphene on a substrate. Due to the interplay between carbon-carbon and carbon-substrate forces, the carbon atoms in the graphene layer are shifted from their regular positions. These static substrate-induced displacements are described by the vector set $(\mathbf{r}_{l0}, z_{l0})$, where the l index spans all atoms, $\mathbf{r}_{l0}$ and z_{l0} are in-plane and out-of-plane displacements correspondingly. Thus we write the following equation for the graphene potential energy:

$$E = \sum_l \left(U_{\text{sub}}(\mathbf{r}_{l0}, z_{l0}) + \sum_j \frac{K(\delta R_{lj})^2}{2} \right), \tag{1}$$

where U_{sub} is the potential energy stemming from the interaction with the substrate, K is the first-neighbor interatomic force constant, and δR_{lj} is the change in distance between lth atom and its neighbors. Here and below, index $j = 1,2,3$ spans the neighbors of an atom. After simple calculations, we get

$$E = \sum_l \left\{ U_{\text{sub}}(\mathbf{r}_{l0}, z_{l0}) + \sum_j \frac{K}{2} \left[(\mathbf{e}_{lj}(\mathbf{r}_{l0} - \mathbf{r}_{j0}))^2 + \frac{\left((z_{l0} - z_{j0})^2 + \left(r^\tau_{l0} - r^\tau_{j0}\right)^2\right)^2}{4R^2} \right] \right\}, \tag{2}$$

Here, $\mathbf{e}_{lj}$ is a unit vector along the direction from atom l to its neighbor j, r^τ is a perpendicular to the bond in-plane displacement, explicitly $r^\tau_{l0} - r^\tau_{j0} = |(\mathbf{r}_{l0} - \mathbf{r}_{j0}) - (\mathbf{e}_{lj} \cdot (\mathbf{r}_{l0} - \mathbf{r}_{j0}))\mathbf{e}_{lj}|$. The positions of the carbon atoms on the amorphous substrate satisfy standard equations for classical energy minima ($\partial E/\partial \mathbf{R}_l = 0$). Introducing small deviations x_l, y_l, z_l from equilibrium positions, we get a perturbation of the conventional in-plane phonon Hamiltonian:

$$\delta H_{\text{in-plane}} = \sum_l \left[\frac{1}{2} \frac{\partial^2 U_{\text{sub}}}{\partial x^2}(\mathbf{r}_{l0}, z_{i0}) x_l^2 + \frac{1}{2} \frac{\partial^2 U_{\text{sub}}}{\partial y^2}(\mathbf{r}_{l0}, z_{i0}) y_l^2 + \sum_j \frac{K\left(r^\tau_l - r^\tau_j\right)^2}{4R^2} \left(3\left(r^\tau_{l0} - r^\tau_{j0}\right)^2 + (z_{l0} - z_{j0})^2\right) \right]. \tag{3}$$

Also, we get the following perturbation for ZA phonons:

$$\delta H_{ZA} = \sum_l \left[\frac{1}{2} \frac{\partial^2 U_{\text{sub}}}{\partial z^2}(\mathbf{r}_{l0}, z_{l0}) z_l^2 + \sum_j \frac{K(z_l - z_j)^2}{4R^2} \left(3(z_{l0} - z_{j0})^2 + (r^\tau_{l0} - r^\tau_{j0})^2\right) \right]. \tag{4}$$

The MD simulation described below allows to obtain the equilibrium structure of graphene on the substrate for temperature $T = 0$ K and the corresponding values of atomic displacements $\mathbf{r}_{l0}$ and z_{l0}. The simulation shows that here the terms with z_{l0} are much larger than the ones with r^τ_{l0}. An extra difference in prefactor 3 allows to omit the terms with r^τ_{l0} here, which is reflected in the definition of parameters β_{lj} in the beginning of Sec. II C.

B. Theory for LA and TA phonons

The perturbation Hamiltonian for the in-plane phonons has the following form [cf. Eq. (3)]:

$$\mathcal{V} = \sum_l \left[\frac{\gamma_l r_l^2}{2} + \sum_j \frac{\xi_{lj}\left(r^\tau_l - r^\tau_j\right)^2}{2} \right]. \tag{5}$$

The parameters γ_l and ξ_{lj},

$$\gamma_l = \frac{\partial^2 U_{\text{sub}}}{\partial x^2}(\mathbf{r}_{l0}, z_{l0}) + \frac{\partial^2 U_{\text{sub}}}{\partial y^2}(\mathbf{r}_{l0}, z_{l0}), \tag{6}$$

$$\xi_{lj} = \frac{K\left(3\left(r^\tau_{l0} - r^\tau_{j0}\right)^2 + (z_{l0} - z_{j0})^2\right)}{4R^2}, \tag{7}$$

were determined using MD simulations. Let

$$\gamma = \langle \gamma_l \rangle, \quad \tilde{\gamma}_l = \gamma_l - \gamma, \tag{8}$$

$$\xi = \langle \xi_{lj} \rangle, \quad \tilde{\xi}_{lj} = \xi_{lj} - \xi, \tag{9}$$

where the angle brackets denote the averaging over disorder configurations. Obviously $\langle \tilde{\gamma}_l \rangle, \langle \tilde{\xi}_{lj} \rangle = 0$. So we can divide

perturbation (5) in two parts:

$$\mathcal{V} = \mathcal{V}_1 + \mathcal{V}_2, \tag{10}$$

$$\mathcal{V}_1 = \gamma \sum_l \left[\frac{r^2}{2} + \xi \sum_j \frac{(r^\tau - r^\tau)^2}{2} \right], \tag{11}$$

$$\mathcal{V}_2 = \sum_l \left[\frac{\tilde{\gamma}_l r_l^2}{2} + \sum_j \frac{\tilde{\xi}_{lj}\left(r_l^\tau - r_j^\tau\right)^2}{2} \right]. \tag{12}$$

It is easy to include $\mathcal{V}_1$ to the exact phonon spectrum, because it only shifts the system vibrational eigenvalues (ω^2) by γ and slightly renormalizes the sound speed c. One can see that the term with ξ in V_1 contains an additional factor $(\mathbf{e}_k - (\mathbf{e}_k \cdot \mathbf{e}_\nu)\mathbf{e}_\nu)^2$, where $\nu = 1,2,3$ indicates the bond index and the phonon wave-vector direction $\mathbf{e_k} = \frac{\mathbf{k}}{k}$. At small momenta k, its average over the momentum angle is almost $1/4$, with a negligible trigonal warping. Thus, in the Debye model, the bare phonon spectrum reads

$$\omega_k = \sqrt{\frac{\gamma}{m} + \left(1 + \frac{\xi}{2K}\right)c^2k^2}, \tag{13}$$

where m is the carbon atom mass. From this expression, one can see that the bare spectrum is gapped. Let $\tilde{c}$ be the renormalized sound speed,

$$\tilde{c} = c\sqrt{\left(1 + \frac{\xi}{2K}\right)}. \tag{14}$$

We use the conventional quantized atom displacement representation:

$$r_l(\mathbf{R}_l,t) = \frac{1}{\sqrt{2mN}} \sum_k \frac{\mathbf{p}_k}{\sqrt{\omega_k}} \left(b_k e^{i\mathbf{k}\mathbf{R}_l} + b_k^+ e^{-i\mathbf{k}\mathbf{R}_l}\right), \tag{15}$$

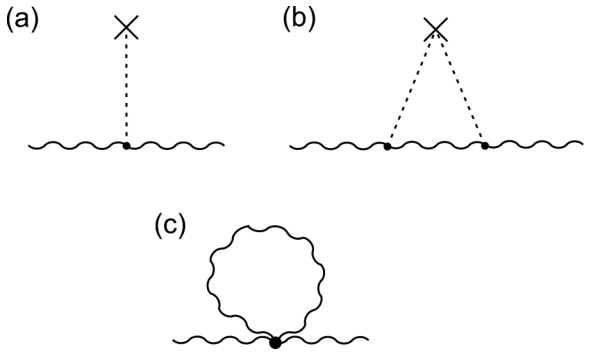

FIG. 1. Diagrams giving corrections to the phonon spectrum. (a) First order in disorder strength correction, which gives zero due to disorder parameters definitions [see, e.g., Eq. (8)], (b) the second-order correction, which is nonzero when the scattering is taking place on the same defect. The waved line is for the phonon Green's function and the dashed line is for the perturbing potential. (c) Correction to ZA phonon spectrum due to phonon-phonon interaction.

where N is the number of unit cells in the system, b_k and b_k^+ are bosonic operators, and $\mathbf{p}_k$ is the phonon polarization. For LA phonons, $\mathbf{p}_k = \mathbf{e}_k$ and for TA phonons $\mathbf{p}_k$ is perpendicular to $\mathbf{e}_k$ and lies in the graphene plane. Using this equation, it is easy to show that

$$\mathcal{H}_0 = \sum_k \omega_k \left(b_k^+ b_k + \frac{1}{2}\right), \tag{16}$$

as in the case of standard gapless acoustic phonons. Using Eq. (15), we have the first part of perturbation (12) in the following form:

$$\mathcal{V}_2 = \frac{1}{4mN} \sum_l \sum_{k_1,k_2} \frac{\mathbf{p}_{k_1} \cdot \mathbf{p}_{k_2} \tilde{\gamma}_l}{\sqrt{\omega_{k_1}\omega_{k_2}}} \left(b_{k_1} b_{k_2} e^{i(\mathbf{k}_1+\mathbf{k}_2)\mathbf{R}_l} + b_{k_1}^+ b_{k_2} e^{i(\mathbf{k}_2-\mathbf{k}_1)\mathbf{R}_l}\right) + \text{H.c.}, \tag{17}$$

where "H.c." is for Hermitian conjugate. A simple estimation shows that the main impact to phonon spectrum stems from normal terms in the perturbation and anomalous terms can be omitted. So including the second part of perturbation (12) yields

$$\mathcal{V}_2 = \frac{1}{2mN} \sum_l \sum_{k_1,k_2} \frac{b_{k_1}^+ b_{k_2} e^{i(\mathbf{k}_2-\mathbf{k}_1)\mathbf{R}_l}}{\sqrt{\omega_{k_1}\omega_{k_2}}} \left\{ \tilde{\gamma}_l \left(\mathbf{p}_{k_1} \cdot \mathbf{p}_{k_2}\right) + \sum_j \left[\tilde{\xi}_{lj} \left(\mathbf{p}_{k_1} - \left(\mathbf{p}_{k_1} \cdot \mathbf{e}_{lj}\right)\mathbf{e}_{lj}\right) \right.\right.$$
$$\left.\left. \cdot \left(\mathbf{p}_{k_2} - \left(\mathbf{p}_{k_2} \cdot \mathbf{e}_{lj}\right)\mathbf{e}_{lj}\right)(1 - e^{-i\mathbf{k}_1(\mathbf{R}_j-\mathbf{R}_l)})(1 - e^{i\mathbf{k}_2(\mathbf{R}_j-\mathbf{R}_l)}) \right] \right\}. \tag{18}$$

In the following calculations, we use this definition for the phonon Green's function:

$$D_0(\omega,\mathbf{k}) = \frac{2\omega_k}{\omega^2 - \omega_k^2 + i0}. \tag{19}$$

The first order in disorder strength correction to the phonon self-energy part is given by the following equation [see Fig. 1(b)]:

$$\Sigma^{(1)}(\omega,\mathbf{k}) = \frac{1}{2m\omega_k} \left\{ \frac{1}{N} \sum_l \left[\tilde{\gamma}_l + \sum_j 2\tilde{\xi}_{lj}(1 - \cos\mathbf{k} \cdot \mathbf{e}_{lj})(\mathbf{p}_k - (\mathbf{p}_k \cdot \mathbf{e}_{lj})\mathbf{e}_{lj})^2) \right] \right\} = 0, \tag{20}$$

because the expression in the brackets contains $\langle\tilde{\gamma}_l\rangle$ and $\langle\tilde{\xi}_{lj}\rangle$, which are zero. The second-order correction is given by the diagram shown in Fig. 1(b). Let us first consider only the term with $\tilde{\gamma}_l$, as the other terms are negligible at small momenta and have no

divergences. The corresponding equation reads

$$\Sigma^{(2)}(\omega,\mathbf{k}) = \frac{1}{4m^2N^2\omega_k}\sum_{l,j}\tilde{\gamma}_l\tilde{\gamma}_j\sum_q \frac{(\mathbf{p}_k\cdot\mathbf{p}_q)^2 D_0(\omega,\mathbf{k})}{\omega_q} e^{i(\mathbf{k}-\mathbf{q})(\mathbf{R}_l-\mathbf{R}_j)}. \tag{21}$$

After averaging over disorder one gets

$$\Sigma^{(2)}(\omega,\mathbf{k}) = \frac{\langle\tilde{\gamma}_l^2\rangle v_0}{2m^2\omega_k}\int\frac{d^2q}{(2\pi)^2}\frac{(\mathbf{p}_k\cdot\mathbf{p}_q)^2}{\omega^2-\omega_q^2+i0}, \tag{22}$$

where v_0 is the unit cell area. To derive the spectrum correction, one should put $\omega=\omega_k$ from Eq. (13) and integrate

$$\int\frac{d^2q}{(2\pi)^2}\frac{(\mathbf{p}_k\cdot\mathbf{p}_q)^2}{k^2-q^2+i0} = \frac{1}{4\pi}\int_0^{k_D}\frac{qdq}{k^2-q^2+i0} \approx \frac{1}{8\pi}\left(\ln\frac{k^2}{k_D^2-k^2}-i\pi\right), \tag{23}$$

where k_D is the Debye wave vector. In our dimensionless notations, it is equal to π. Thus the self-energy reads

$$\Sigma_\gamma^{(2)}(\omega_k,\mathbf{k}) = \frac{\langle\tilde{\gamma}_l^2\rangle v_0}{16\pi m^2\tilde{c}^2\omega_k}\left(\ln\frac{k^2}{k_D^2-k^2}-i\pi\right). \tag{24}$$

Renormalized spectrum can be found from the following equation:

$$\frac{1}{D(\omega,\mathbf{k})} = \frac{1}{D_0(\omega,\mathbf{k})} - \Sigma^{(2)}(\omega_k,\mathbf{k}) = 0, \tag{25}$$

which has the following solution:

$$\Omega_k = \omega_k\sqrt{1+\frac{\langle\tilde{\gamma}_l^2\rangle v_0}{8\pi m^2\tilde{c}^2\omega_k^2}\left(\ln\frac{k^2}{k_D^2-k^2}-i\pi\right)}. \tag{26}$$

The logarithmic divergencies of this spectrum show that for large enough graphene sheets of the size $L\gg 0.1$ mm, the phonons at the bottom and at the top of the band are localized due to the scattering on disorder. However, for actual sizes of graphene sheets, this is not the case.

Also, there are corrections to phonon spectrum from perturbation (18), which are negligible at small momenta, but can play a significant role out of the long-wavelength region. MD analysis shows that the most important correction is the one containing $\tilde{\xi}_{lj}^2$. The corresponding equation reads

$$\Sigma_\xi^{(2)}(\omega_k,\mathbf{k}) = \sum_j\frac{32\langle\tilde{\xi}_{lj}^2\rangle v_0\sin^2\frac{k_j}{2}}{m^2\tilde{c}^2\omega_k}\int\frac{d^2q}{(2\pi)^2}\frac{((\mathbf{p}_k-(\mathbf{p}_k\cdot\mathbf{e}_j)\mathbf{e}_j)\cdot(\mathbf{p}_q-(\mathbf{p}_q\cdot\mathbf{e}_j)\mathbf{e}_j))^2\sin^2\frac{q_j}{2}}{k^2-q^2+i0}, \tag{27}$$

where k_j and q_j are projections of wave vectors $\mathbf{k}$ and $\mathbf{q}$ on the bond direction $\mathbf{e}_j$ with the jth atom. So for the in-plane phonons, the self-energy part of the scattering on disorder has the following form:

$$\Sigma_{LA}^{(2)}(\mathbf{k}) = \Sigma_\gamma^{(2)}(\omega_k,\mathbf{k}) + \Sigma_\xi^{(2)}(\omega_k,\mathbf{k}), \tag{28}$$

and the equation for the phonon spectrum valid in the whole Brillouin zone reads

$$\Omega_k = \omega_k\sqrt{1+2\Sigma_{LA}^{(2)}(\mathbf{k})/\omega_k}. \tag{29}$$

The phonon lifetime due to scattering by the substrate-induced disorder can be extracted from the spectra as its imaginary part $\tau_{\text{substr}}^{-1}(k)=\Im\{\Omega_k\}$. The only difference in derivations between LA and TA phonons is in polarizations in Eq. (27).

C. Theory for ZA phonons

For ZA phonons, one can see from expression (4) that we have two different perturbation parts. So let us introduce two sets of parameters, which can be calculated from MD simulations:

$$\alpha = \left\langle\frac{\partial^2 U_{\text{sub}}}{\partial z^2}(\mathbf{r}_{l0},z_{l0})\right\rangle, \tag{30}$$

$$\alpha_l = \frac{\partial^2 U_{\text{sub}}}{\partial z^2}(\mathbf{r}_{l0},z_{l0}) - \alpha, \tag{31}$$

$$\beta = \left\langle\frac{3K}{4R^2}(z_{l0}-z_{j0})^2\right\rangle, \tag{32}$$

$$\beta_{lj} = \frac{3K}{4R^2}(z_{l0}-z_{j0})^2 - \beta. \tag{33}$$

Obviously $\langle\alpha_l\rangle=\langle\beta_{lj}\rangle=0$. The regular translationally invariant part of the Hamiltonian has the following form:

$$\mathcal{H}_{ZA}^{(0)} = \sum_i\left[\frac{p_{zi}^2}{2m}+\frac{\alpha z_i^2}{2}+\sum_j\frac{\beta(z_i-z_j)^2}{2}\right]. \tag{34}$$

Comparing this Hamiltonian with the conventional one for suspended graphene one can see that the spectrum is given by

$$\omega_k = \sqrt{\frac{\alpha}{m}+c_{ZA}^2k^2}, \tag{35}$$

where

$$c_{ZA} = \left(\frac{2\beta}{K}\right)^{1/2}c. \tag{36}$$

It is instructive to compare the obtained dispersion of flexural phonons with the one from the paper by Amorim and Guinea [49]. First, both dispersions are gapped with a gap width controlled by the strength of graphene-substrate interaction α, which defines the minimal vibration energy in the field of the substrate (cf. with g parameter from Ref. [49]). The difference is in the power of the phonon wave vector q. Amorim and Guinea consider the quadratic in displacement

intrinsic bending rigidity of graphene for restoring force and as a result the dispersion is quadratic for large q. On the contrary, as one sees from Eq. (34), here the quadratic in displacement force associated with β terms plays the role of restoring force. It results in a linear bare specrtrum of flexural phonons for graphene on substrate for large q, which significantly differs from the spectrum of freestanding graphene and graphene on crystalline substrate. In fact, the dispersion of ZA phonons of graphene on an amorphous substrate has rather extrinsic than intrinsic origin.

As the phonon-phonon interaction is significant in the case of ZA phonons, we consider the anharmonic term in the Hamiltonian,

$$V = U\sum_{l,j}(z_l - z_j)^4, \tag{37}$$

where summation is conducted over all nearest neighbors, and $U = K/8R^2$. In quantized form,

$$V = \frac{3U}{2m^2N}\sum_{k_1+k_2=k_3+k_4}\frac{b^+_{k_1}b^+_{k_2}b_{k_3}b_{k_4}}{\sqrt{\omega_{k_1}\omega_{k_2}\omega_{k_3}\omega_{k_4}}} \times \sum_j(1-e^{-ik_{1j}})(1-e^{-ik_{2j}})(1-e^{ik_{3j}})(1-e^{ik_{4j}}). \tag{38}$$

$k_{1j},k_{2j},k_{3j},k_{4j}$ are the projections of wave vectors $\mathbf{k}_1,\mathbf{k}_2,\mathbf{k}_3,\mathbf{k}_4$ on the direction from an arbitrary atom to its jth neighbor in the real space. A linear in U correction is given by the diagram in Fig. 1(c) with the corresponding equation in the Matsubara technique written as

$$\Sigma_T(\mathbf{k}) = \frac{12Kv_0}{2mR^2\omega_k}\sum_j\sin^2\frac{k_j}{2}\int\frac{d^2q}{(2\pi)^2}\frac{\sin^2\frac{q_j}{2}}{\omega_q}\coth\frac{\omega_q}{2T}. \tag{39}$$

Thus the spectrum used henceforth is

$$\omega^T_k = \omega_k\sqrt{1+\frac{2\Sigma_T(\mathbf{k})}{\omega_k}}. \tag{40}$$

The perturbation Hamiltonian has the following form:

$$\mathcal{V} = \sum_l\left[\frac{\alpha_l z_l^2}{2}+\sum_j\frac{\beta_{lj}(z_l-z_j)^2}{2}\right], \tag{41}$$

once again we omit the anomalous terms and rewrite the perturbation:

$$\mathcal{V} = \frac{1}{2mN}\sum_l\sum_{k_1,k_2}\frac{b^+_{k_1}b_{k_2}}{\sqrt{\omega_{k_1}\omega_{k_2}}}e^{i(\mathbf{k}_2-\mathbf{k}_1)\mathbf{R}_l} \times\left[\alpha_l+\sum_j\beta_{lj}(1-e^{-i\mathbf{k}_1(\mathbf{R}_j-\mathbf{R}_l)})(1-e^{i\mathbf{k}_2(\mathbf{R}_j-\mathbf{R}_l)})\right]. \tag{42}$$

At small momenta $k \ll 1$, the second-order spectrum correction is given only by the term with α_l. As in the previous section, this correction is logarithmically divergent for long-wavelength phonons. This indicates their localization at $k \ll a_0/L$, where a_0 is the lattice parameter and L is the graphene flake size. Expressions for all corrections of the second order in disorder strength are presented in Appendix A. Based on the results of MD simulations presented in Sec. II D, we only keep the two main terms producing the highest contributions, which give the following self-energy:

$$\Sigma^{(2)}_{ZA}(\mathbf{k}) = \frac{v_0}{m^2\omega^T_k}\left(\langle\alpha_l^2\rangle I_1(k)+32\langle\beta_{lj}^2\rangle\sum_j\sin^2\frac{k_j}{2}I_{2j}(\mathbf{k})\right), \tag{43}$$

where

$$I_1(\mathbf{k}) = \frac{1}{2}\int\frac{d^2q}{(2\pi)^2}\frac{1}{\left(\omega^T_k\right)^2-\left(\omega^T_q\right)^2+i0}, \tag{44}$$

$$I_{2j}(\mathbf{k}) = \int\frac{d^2q}{(2\pi)^2}\frac{\sin^2\frac{q_j}{2}}{\left(\omega^T_k\right)^2-\left(\omega^T_q\right)^2+i0}. \tag{45}$$

The corresponding expression for the ZA phonon spectrum reads

$$\Omega_k = \omega^T_k\sqrt{1+2\Sigma^{(2)}_{ZA}(\mathbf{k})/\omega^T_k}. \tag{46}$$

D. Molecular dynamics simulation

The GROMACS [50] package was used to perform all MD simulations. The 72 Å×72 Å×36 Å amorphous SiO_2 substrate consisting of 12 000 atoms was rigid. The round graphene sheet of diameter $D \approx 40$ Å consisted of 481 carbon atoms. The C-C interactions within the graphene sheet were modeled with a harmonic potential $K = 27$ eV/Å^2, which corresponds to the first-neighbor interatomic force constant from Ref. [51]. This model is consistent with the employed analytical description of graphene vibrational properties. The interactions between the C atoms of graphene and the Si and O atoms of the substrate were modeled with a Lennard-Jones potential with parameters taken from Ref. [44].

The graphene sheet initial position was 1 Å above the substrate. The simulation was performed with a 0.02-ps time step, and the temperature was controlled with a weak coupling algorithm [52]. During the first 500 ps, the graphene sheet was attracted by the substrate and started planar diffusion on its surface. Then, from the initial value of 300 K, the temperature was lowered to zero for 500 ps using velocity rescale temperature coupling [52].

The obtained freezed equilibrium configuration of graphene on a SiO_2 substrate was treated in MATHEMATICA [53] package to derive the parameters required by the theory. Only carbon atoms with three neighbors were considered. The results exhibit no significant dependence on the initial conditions of MD simulations. The required by the perturbation theory

TABLE I. The obtained with MD parameters required by perturbation theory. All values are given in eV/Å^2.

In-plane phonons				ZA phonons			
γ	$\sqrt{\langle\tilde{\gamma}_l^2\rangle}$	ξ	$\sqrt{\langle\xi_{lj}^2\rangle}$	α	$\sqrt{\langle\alpha_l^2\rangle}$	β	$\sqrt{\langle\beta_{lj}^2\rangle}$
0.006	0.015	0.2	0.28	0.09	0.11	0.59	0.82

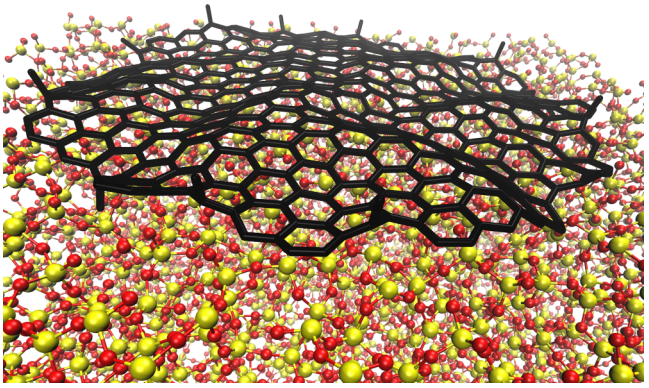

FIG. 2. The final structure of graphene on amorphous SiO_2 obtained with MD simulations.

graphene-substrate interaction energy parameters are listed in Table I. Figure 2 shows the obtained geometry of graphene on the amorphous SiO_2 substrate. The obtained value of $\beta = 0.09$ eV/Å^2 corresponds to the graphene-substrate coupling parameter $g = 5\times10^{19}$ J/m^4, which is four times smaller than the estimation from Ref. [54]. This is due to not complete slippage between the graphene sheet and the rough amorphous SiO_2 substrate.

The atomic Z coordinate root mean square displacement for graphene on the substrate with respect to the initial unperturbed graphene is 0.04 nm. For the X and Y coordinates, we obtain 0.007 nm. With high accuracy $\beta = 3\xi$ and $\sqrt{\langle\beta_{ij}^2\rangle} = 3\sqrt{\langle\xi_{jl}^2\rangle}$.

III. RESULTS AND DISCUSSION

A. Spectra and relaxation times of ZA phonons

As it was discussed above, the bare spectrum of ZA phonons for graphene on a disordered substrate given by Eq. (35) differs from the one for freestanding graphene and graphene on a crystalline substrate given by $\omega_k = Ak^2$, where $A \approx 3.1 \times 10^{-3}$ cm^2 s^{-1} [55]. The phonon-phonon interaction described by (40) leads to the effective increasing of c_{ZA}. For $T = 300$ K the value of c_{ZA} is 6 km/s or approximately 30% of the in-plane phonon velocity. Figure 3(a) shows the real and the imaginary parts of ZA phonon spectrum for $T = 300$ K calculated with Eq. (46) using parameters from Table I and Fig. 3(b) shows the ZA phonon spectrum imaginary to real part ratio.

In the considered system, we have strong disorder for ZA phonons with spectrum ω_k^T calculated via Eq. (40). It is well known that even disorder with small concentration leads to localization of long-wavelength excitations (for bosonic systems see, e.g., Refs. [56–58]). However, here the "impurities concentration" is equal to 1, providing spectrum corrections of the order of the pure spectrum (40) in the whole Brillouin zone [see Fig. 3(a)], which makes ZA phonons overdamped [see Fig. 3(b)] and their nature becomes a question of further considerations, hence a possible scenario is the localization of all ZA phonon modes. Anyway, from our theory it is quite natural to make a conclusion that ZA phonons do not contribute to the heat conductivity of graphene on an amorphous substrate.

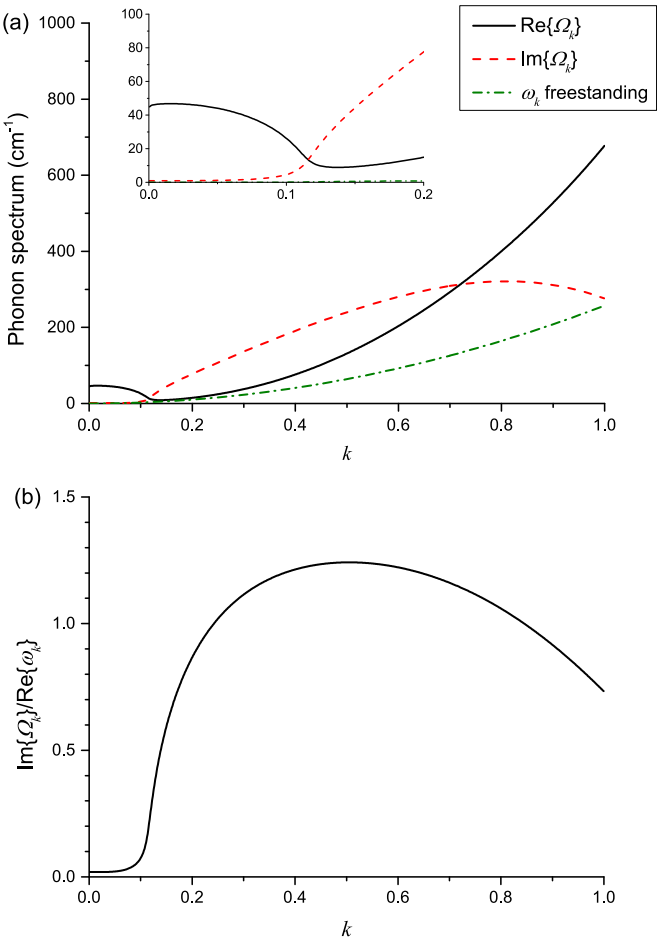

FIG. 3. (a) Calculated spectrum of ZA phonons in graphene on an amorphous substrate. Solid black curve and red dashed curves are for the real and the imaginary parts of the ZA phonon spectrum at $T = 300$ K for graphene on an amorphous substrate, respectively. The green dash-dot curve is for the ZA phonon spectrum of freestanding graphene. (b) The ratio of the imaginary part of the ZA phonon spectra to the real part of the bare spectra for graphene on a disordered substrate.

B. Phonon scattering mechanisms in graphene

To understand the impact of the substrate on the graphene heat conductivity, it is necessary to compare the phonon scattering on the substrate-induced disorder with other mechanisms of phonon relaxation in graphene. The conventional mechanisms of phonon lifetime reduction in graphene are scattering on the graphene flake boundaries and anharmonic three-phonon scattering processes, while point defect scattering is weak compared to other mechanisms. The single-mode relaxation time approximation (SMRTA) is always used to describe the boundary scattering and the corresponding phonon lifetime can be written as $\tau_L^{-1} = v_k/L$, where $v_k = \frac{\partial\omega_k}{\partial k}$ is the phonon group velocity, and L estimates the graphene sample size. For the in-plane phonons, the averaged sound velocity can be taken without loss of accuracy.

Currently, there is no established theory on the suspended graphene heat conductivity due to the complexity of the anharmonic processes. Various approaches including usage of BTE within SMRTA [33], exact iterative solution of

BTE accounting for three-phonon scattering [47,48], and MD simulations [59] yield different values of graphene heat conductivity κ and the distribution of the heat flux between LA, TA, and ZA modes. The relevant data are accumulated in Table III from the review in Ref. [13].

The contribution of anharmonic processes to phonon damping can be described within the SMRTA with the power law [33,60,61]

$$\tau_{\text{anh}}^{-1} = (B_N + B_U \exp(-\Theta/BT))\omega^2 T^3, \tag{47}$$

where T is the temperature, ω is the phonon frequency, $\Theta \approx 1000$ K is the Debye temperature, $B = 3$, $B_N = B_U/2$, and $B_U = 7.7\times10^{-25}$ s K^{-3}, see Ref. [33].

Recently, it was shown that the approach for considering anharmonic processes in graphene, which reflects all peculiarities of three-phonon scattering should look beyond SMRTA. This problem requires an exact solution of BTE for the three-phonon scattering. In this model, the strong mixing of the in-plane and the flexural phonon modes was justified by Linsay *et al.* [47]. The authors show that the selection rules for the phonon decay include necessary involvement of even number of flexural phonons. The direct LA,TA $\rightarrow$ ZA + ZA and inverse processes ZA + ZA $\rightarrow$ LA,TA provide a balance between in-plane and flexural phonon distribution functions. To calculate the value of heat conductivity, authors relate an effective relaxation time for each phonon mode from the obtained distribution function correction. A contribution of ZA phonons to the free-standing graphene heat conductivity of about 80% in a wide temperature range was reported. Another result of this study is that SMRTA and exact BTE solutions give 2–3 times discrepancy in κ magnitude for LA and TA modes (up to 8 times for ZA mode [47]). Singh *et al.* in Ref. [48] use a similar approach and also conclude that ZA phonons give significant contribution to κ. The authors give an estimate of the total phonon lifetime, which differs from the result of the SMRTA approach up to 3 orders of magnitude. They also show that the lifetime of the in-plane phonons with respect to conversion to the ZA mode is twice longer than the total lifetime.

The following two approaches were used to estimate the value of τ_{anh} for deriving the graphene heat conductivity κ estimation. First, τ_{anh} was calculated by formula (47), see Ref. [33]. Second, it was adopted from Ref. [48], see Fig. 6 there.

The interaction with the substrate will affect the selection rules for phonon scattering. The localization of flexural phonons (see Sec. III A) can change the distribution of the heat flux between LA, TA, and ZA modes. Without understanding the nature of localized ZA phonons in graphene on an amorphous substrate one can not make any judgement about the mixing of in-plane and ZA phonons, which opens a field for further investigations.

The total phonon relaxation time was estimated via Matthiessen's rule $\tau_{\text{total}}^{-1} = \tau_L^{-1} + \tau_{\text{anh}}^{-1} + \tau_{\text{substr}}^{-1}$. The estimation of the contribution to graphene heat conductivity from a given phonon mode can be written as

$$\kappa = \frac{\hbar}{h}\int k dk \tau_{\text{total}}(k)\omega_k \frac{\partial N^0(\omega_k)}{\partial T} v_k^2, \tag{48}$$

where $N^{(0)}$ is equilibrium Bose distribution function and $h = 0.335$ nm is the graphene layer thickness.

Athough ZA phonons are localized, calculating the ZA phonon contribution to thermal conductivity using Eq. (48), where one assumes $v_k = \frac{\partial}{\partial k}\Re\{\Omega_k\}$ and $\tau_{\text{substr}}^{-1} = \Im\{\Omega_k\}$, yields less than 20 W m^{-1} K^{-1}. The contribution of ZA phonons can be thus anyway neglected due to significant reduction of lifetime. Figure 3(a) with the characteristic magnitude of ZA phonon spectrum imaginary part shows that τ_{substr} is lower than 0.1 ps in most volume of Brillouin zone.

C. Spectra and relaxation times of in-plane phonons

The substrate influence on the in-plane phonons in graphene constitutes in the following effects. First, according to Eq. (13), the interaction with the substrate leads to an opening of band gap of $\approx$22 K, see Fig. 4. It results in a phonon occupation number suppression for low temperatures and a corresponding reduction of graphene thermal conductivity for temperatures lower than 20 K.

Secondly, the scattering by the substrate-induced disorder leads to additional reduction of phonon lifetime. The predictions on the strength of this effect strongly depend on the model for τ_{anh} employed. So for τ_{anh} calculated by Eq. (47) both in suspended and supported graphene, the boundary scattering is the dominant mechanism of long wavelength phonon damping and defines the heat conductivity at low temperatures. At low temperatures, only long wavelength phonons are excited and give contribution to heat conductivity. On the contrary, for τ_{anh} adopted from Ref. [48], such phonons are damped due to anharmonic processes. For shorter wavelength phonons, which are excited at temperatures above 100 K, the dominant mechanism corresponds to the anharmonic processes and to substrate-induced disorder scattering.

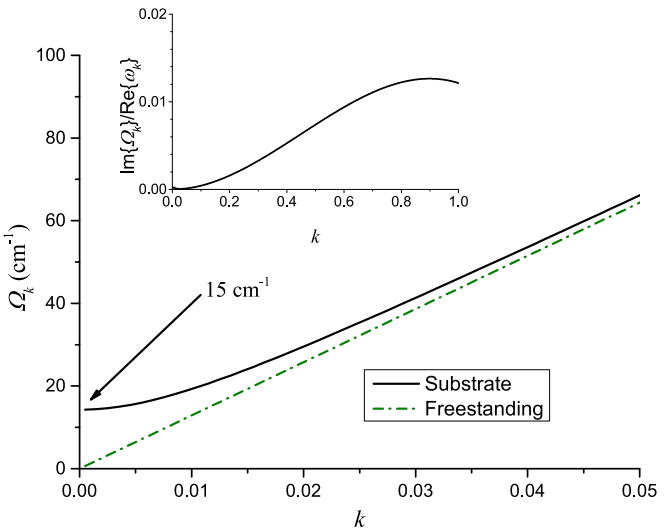

FIG. 4. Dispersion relations of in-plane acoustic phonons in freestanding graphene and in graphene on a substrate. The inset shows the LA phonon spectrum imaginary to real part ratio for graphene on a disordered substrate. The phonon wave vector k is given in units of π/a_0 and $k = 1$ corresponds to the boundary of the Brillouin zone.

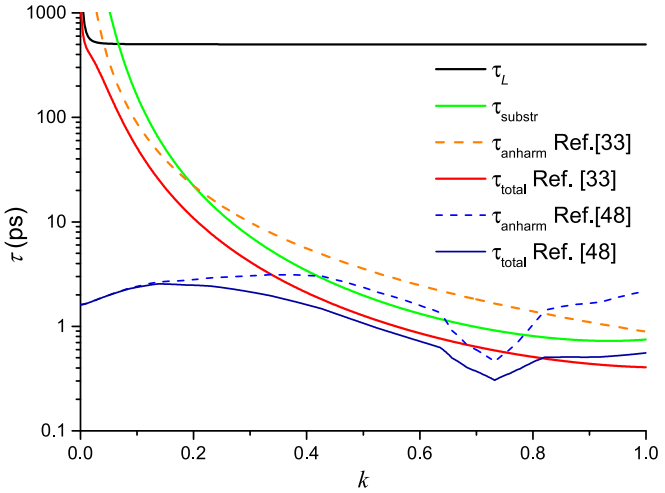

FIG. 5. LA phonons relaxation times corresponding to various mechanisms of scattering. Black solid curve is for relaxation time related to boundary scattering τ_L with $L = 10$ μm. Green solid curve is for substrate-induced phonon damping. Orange dashed curve is for anharmonic processes for temperature $T = 300$ K obtained by Eq. (47) and solid red curve is for total phonon lifetime in this model, derived with Matthiessen's rule. The light blue dashed curve is for τ_{anh} at $T = 300$ K adopted from Ref. [48] and the blue solid curve is for the corresponding total lifetime.

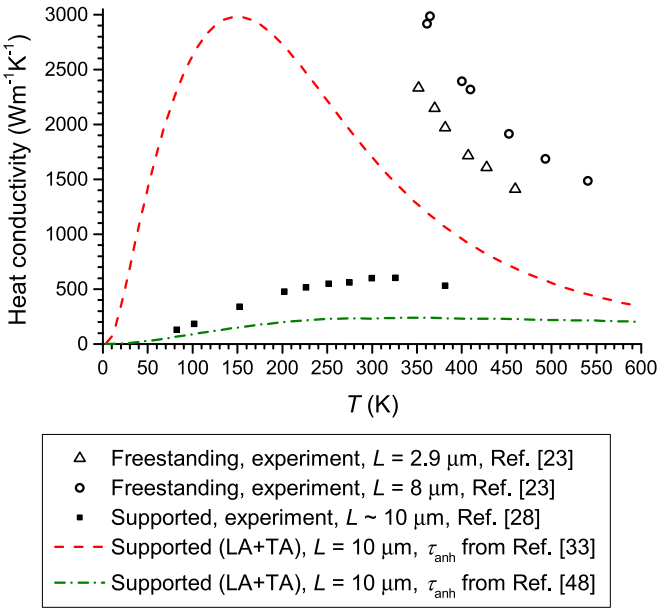

FIG. 6. Experimental data on the heat conductivity of freestanding graphene for $L = 2.9$ μm (open triangles), $L = 8$ μm (open circles) [25], and the heat conductivity of graphene on an amorphous substrate (black solid squares) [30]. The red dashed curve denotes heat conductivity of graphene on an amorphous substrate calculated with BTE as a sum of LA and TA phonons contributions with τ_{anh} given by Eq. (47) (see Ref. [33]). Green dash-dot curve is for the same but with τ_{anh} adopted from Ref. [48].

Figure 5 shows the dependence of the relaxation time of LA phonons on the phonon wave vector magnitude for various mechanisms. The phonon lifetime for anharmonic processes is given for 300 K. For TA phonons, the effect of the substrate is weaker due to polarization effects stemming from integral (27) and anharmonic processes are more important than the substrate effect.

The obtained values of the in-plane phonon lifetime yield the phonon drag thermopower at the level of several μV K^{-1}, which is much smaller than the diffusion contribution to thermopower [23].

D. Graphene heat conductivity

As it was shown above, the graphene-substrate interaction suppresses the contribution of ZA phonons to heat conductivity in the whole range of temperatures for graphene bonded with an amorphous SiO_2 substrate. This contribution is negligible due to ZA phonon localization and extremely short lifetime. Therefore, the total heat conductivity is governed by in-plane phonons.

The behavior of heat conductivity depends on the applied model for τ_{anh} estimation. For the τ_{anh} given by Eq. (47), at temperatures below 100 K, the in-plane phonon heat conductivity is governed by boundary scattering for both supported and suspended graphene. For τ_{anh} adopted from Ref. [48], the anharmonic processes play the main role at temperatures below 100 K. At temperatures above 100 K, the dominant mechanism corresponds to the anharmonic processes and to substrate-induced disorder scattering in both models for supported graphene. As a result, the supported graphene heat conductivity is several times smaller than for freestanding graphene, which is in a qualitative agreement with available experimental data.

For τ_{anh} adopted from Ref. [48] in the whole temperature range, the anharmonic processes give the main contribution to LA and TA phonon damping (see Fig. 5), at the same time, the flexural phonons contribution in this model reaches 90%. Thus due to localization of flexural phonons, the reduction of supported graphene heat conductivity is drastic. Figure 6 shows the experimentally measured heat conductivity of freestanding and supported graphene and the corresponding theoretical predictions based on the developed perturbation theory and BTE. Experimental data from Ref. [30] indicate a significant suppression of the supported graphene heat conductivity below 300 K and a shift of the maximum from $\approx$200 K for freestanding graphene to 300 K.

Using τ_{anh} from Eq. (47) leads to a serious overestimation of heat conductivity, especially at low temperatures. As it can be seen from Fig. 7(a) to bring theory in agreement with the experiment, the assumption $L = 0.2$ μm is sufficient, whereas the experiment yields a graphene sheet size of several micrometers.

On the contrary, taking τ_{anh} adopted from Ref. [48] leads to twofold underestimation of supported graphene heat conductivity. In this model, the heat conductivity does not significantly depend on the graphene flake size L for $L > 0.5$ μm, see Fig. 7(b).

Alternatively, to explain the observed experimental behavior of heat conductivity, the authors of Ref. [30] develop a theory based on the Fermi golden rule and apply Klemens formalism [37] to the case of a large area spot contact between

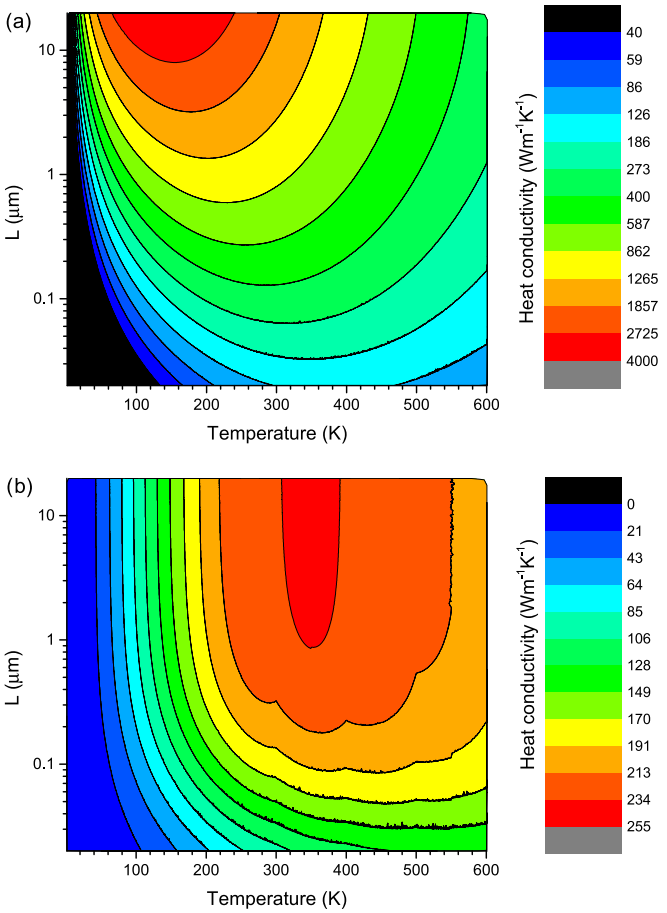

FIG. 7. The obtained within the developed theory dependence of supported graphene heat conductivity on temperature T and size L. For (a) the τ_{anh} was estimated with Eq. (47) (see Ref. [33]) and for (b) τ_{anh} was adopted from Ref. [48].

graphene and substrate. In their model, the suppression of long wavelength phonon lifetimes stems from an arguable assumption of a constant phonon scattering matrix element. The conventional form of the matrix element given in Ref. [37] is quadratic in the phonon frequency, which yields suppression of high frequency phonons instead, see Eq. (32) in Ref. [36].

It is also necessary to compare the obtained data on the phonon lifetimes and graphene thermal conductivity with results of the MD simulations. Figure 2 from Ref. [44] shows that the lifetime of both in-plane and ZA phonons in suspended graphene lies in the range from 10 to 25 ps. For supported graphene, the characteristic lifetimes of all phonon modes are from several picoseconds to 10 ps. These results are in contradiction with the relatively weak effect of the substrate on the in-plane phonons and dramatic suppression of the ZA phonon lifetime predicted here.

Other studies lie in agreement with our predictions. MD simulations performed in Ref. [45] yield 90% reduction of ZA phonon contribution to the thermal conductivity and spectrum deformation for the actual strength of the graphene-substrate interaction, which coincides with the results of the present study. The MD study in Ref. [62] indicates several times reduction of in-plane phonon lifetime and several orders reduction of ZA phonon lifetime in supported graphene, which qualitatively agrees with the present study. Finally, Ref. [40] predicts localization of excitations in amorphous graphene and a corresponding two-fold decrease of heat conductivity.

The predictions on graphene heat conductivity are robust with respect to variation of the energy parameters from Table I. Although we account only for a pair harmonic potential for C-C bonds in MD simulations, we argue that using more sophisticated models (E.G. Tersoff [63] and optimized Tersoff [64] potentials accounting for three-atomic torsional rigidity and potentials accounting for next neighbors interactions [51]) would slightly renormalize the parameters and the obtained qualitative picture remains intact.

The employed model lies in agreement with the fact that graphene sheets conform to the underlying silicon oxide substrate, reported in Refs. [15,65]. However, this model does not account for long-range (20 nm) height correlations of the substrate and graphene. Also these studies report that graphene sheet conforms the substrate corrugations but with smaller amplitude, which is an evidence of graphene being partially suspended. The elucidation of the geometry of graphene interacting via the van der Waals force with amorphous substrates is to be clarified in further experimental studies and MD simulations. The developed model is rather related to the atomically smooth substrates. The considered effect of an amorphous substrate on graphene intrinsic heat conductivity is important when creating graphene-based electronic devices with the heat-sink functions placed on graphene pathways and should be taken into account when managing circuit thermal parameters.

ACKNOWLEDGMENTS

S.K. acknowledges support by the Russian Science Foundation (Project No. 16-19-00075 "Thermoelectric generator with record parameters based on carbon nanostructures: development of scientific bases"). O.U. acknowledges Russian Science Foundation (Project No 14-22-00281 "Low dimensional quantum field theory in elementary particles and condensed matter physics"). I.T. acknowledges Skolkovo Foundation (Grant agreement for Russian educational and scientific organization No. 4dd.25.12.2014 to I.T.). A.N. acknowledges financial support from the EPSRC Established Career fellowship of A. V. Kavokin. The authors are grateful to M. V. Dubina for his attention to the work, to A. V. Syromyatnikov and A. G. Yashenkin for valuable discussions and to E. D. Eidelman for his support.

APPENDIX A: ZA PHONONS SELF-ENERGY PART CORRECTIONS

From (41) we see that in the second order in disorder strength we have different corrections. We treat this perturbation conventionally, considering only the terms with disorder constants corresponds to the same site. Thus we have four terms, proportional to $\langle\alpha_l^2\rangle$, $\langle\beta_{lj}^2\rangle$, $\langle\alpha_l\beta_{lj}\rangle$, and $\langle\beta_{lj}\beta_{lm}\rangle$ for $j \neq m$.

The correction proportional to $\langle\alpha_l^2\rangle$ is logarithmically divergent at very small momenta k and contains the following

integral:

$$I_1(k) = \frac{1}{2}\int \frac{d^2q}{(2\pi)^2}\frac{1}{\left(\omega_k^T\right)^2 - \left(\omega_q^T\right)^2 + i0}. \quad \text{(A1)}$$

The second correction stems from nonzero average $\langle\beta_{lj}^2\rangle$. The corresponding equation is

$$\sum_j \frac{32\langle\beta_{lj}^2\rangle v_0 \sin^2\frac{k_j}{2}}{m^2\omega_k^T}\int \frac{d^2q}{(2\pi)^2}\frac{\sin^2\frac{q_j}{2}}{\left(\omega_k^T\right)^2 - \left(\omega_q^T\right)^2 + i0}, \quad \text{(A2)}$$

where the summation is over three possible neighbor positions and q_j and k_j are the corresponding momenta projections. We denote the corresponding integral as

$$I_{2l}(k) = \int \frac{d^2q}{(2\pi)^2}\frac{\sin^2\frac{q_j}{2}}{\left(\omega_k^T\right)^2 - \left(\omega_q^T\right)^2 + i0}. \quad \text{(A3)}$$

The third correction is due to correlations between α_l and β_{lj}. The corresponding equation is

$$\frac{2v_0\langle\alpha_l\beta_{lj}\rangle}{m^2\omega_k^T}\sum_j\int \frac{d^2q}{(2\pi)^2}\frac{f(\mathbf{k},\mathbf{q},j)}{\left(\omega_k^T\right)^2 - \left(\omega_q^T\right)^2 + i0}, \quad \text{(A4)}$$

where

$$f(\mathbf{k},\mathbf{q},j) = 1 + \cos(k_j - q_j) - \cos k_j - \cos q_j. \quad \text{(A5)}$$

Expression (A4) can be simplified using

$$1 + \cos(k_j - q_j) - \cos k_j - \cos q_j = \sin k_j \sin q_j + 4\sin^2\frac{k_j}{2}\sin^2\frac{q_j}{2}, \quad \text{(A6)}$$

the first term gives zero after integration over the angle, so the correction obeys the following form:

$$\frac{8v_0\langle\alpha_l\beta_{lj}\rangle}{m^2\omega_k^T}\sum_j \sin^2\frac{k_j}{2}\int \frac{d^2q}{(2\pi)^2}\frac{\sin^2\frac{q_j}{2}}{\left(\omega_k^T\right)^2 - \left(\omega_q^T\right)^2 + i0}, \quad \text{(A7)}$$

the corresponding integral denotation is

$$I_{3j}(k) = \int \frac{d^2q}{(2\pi)^2}\frac{\sin^2\frac{q_j}{2}}{\left(\omega_k^T\right)^2 - \left(\omega_q^T\right)^2 + i0}. \quad \text{(A8)}$$

The last correction arises from correlations between β_{ij} and β_{il}, where j and l denote different neighboring sites. The corresponding equation is

$$\sum_{j\neq m}\frac{32\langle\beta_{lj}\beta_{lm}\rangle v_0}{m^2\omega_k^T}\int \frac{d^2q}{(2\pi)^2}\frac{g(\mathbf{k},\mathbf{q},j,m)}{\left(\omega_k^T\right)^2 - \left(\omega_q^T\right)^2 + i0}, \quad \text{(A9)}$$

where

$$g(\mathbf{k},\mathbf{q},j,m) = \cos\frac{(\mathbf{k}-\mathbf{q})(\mathbf{e}_m - \mathbf{e}_j)}{2} \times \sin\frac{k_j}{2}\sin\frac{k_m}{2}\sin\frac{q_j}{2}\sin\frac{q_m}{2}, \quad \text{(A10)}$$

so

$$I_{4jm}(k) = \int \frac{d^2q}{(2\pi)^2}\frac{g(\mathbf{k},\mathbf{q},j,m)}{\left(\omega_k^T\right)^2 - \left(\omega_q^T\right)^2 + i0}. \quad \text{(A11)}$$

The real parts of this expressions are the principal values of the corresponding integrals, and the imaginary parts are

$$\Im\left[\int \frac{d^2q}{(2\pi)^2}\frac{F(\mathbf{k},\mathbf{q})}{k^2 - q^2 + i0}\right] = -\frac{\pi}{(2\pi)^2}\int d\varphi \frac{kF(\mathbf{e}_k,\mathbf{e}_q,q=k)}{\frac{\partial(\omega_q^T)^2}{\partial q}(k)}. \quad \text{(A12)}$$

The obtained with MD simulations values of energy parameters are $\sqrt{\langle\alpha_l\beta_{lj}\rangle} = \sqrt{-0.016}\,\text{eV/Å}^2$ and $\sqrt{\langle\beta_{lj}\beta_{lm}\rangle} = \sqrt{-0.002}\,\text{eV/Å}^2$.

APPENDIX B: APPROXIMATION OF INTEGRAL IN THE IN-PLANE PHONON SELF-ENERGY PART CORRECTION

The integral in Eq. (27) required for calculating $\Sigma_\xi^{(2)}$ and τ_{substr} for TA phonons can be approximated with sufficient accuracy as follows:

$$\sum_j \sin^2\frac{k_j}{2}\int \frac{d^2q}{(2\pi)^2}\frac{((\mathbf{p}_k - (\mathbf{p}_k\cdot\mathbf{e}_j)\mathbf{e}_j)\cdot(\mathbf{p}_q - (\mathbf{p}_q\cdot\mathbf{e}_j)\mathbf{e}_j))^2\sin^2\frac{q_j}{2}}{k^2 - q^2 + i0} \approx 0.2k^2 - 2.2k^3 + 2.33k^4 - i(1.51k^4 - 1.11k^5). \quad \text{(B1)}$$

Its dependence on the direction of $\mathbf{k}$ with respect to graphene bonds is weak. For LA phonons, the integral is four times larger.

[1] I. Frank, D. M. Tanenbaum, A. Van der Zande, and P. L. McEuen, Mechanical properties of suspended graphene sheets, J. Vac. Sci. Technol. B **25**, 2558 (2007).

[2] C. Lee, X. Wei, J. W. Kysar, and J. Hone, Measurement of the elastic properties and intrinsic strength of monolayer graphene, Science **321**, 385 (2008).

[3] A. H. Castro Neto, F. Guinea, N. M. R. Peres, K. S. Novoselov, and A. K. Geim, The electronic properties of graphene, Rev. Mod. Phys. **81**, 109 (2009).

[4] S. Das Sarma, S. Adam, E. H. Hwang, and E. Rossi, Electronic transport in two-dimensional graphene, Rev. Mod. Phys. **83**, 407 (2011).

[5] E. H. Hwang, S. Adam, and S. Das Sarma, Carrier Transport in Two-Dimensional Graphene Layers, Phys. Rev. Lett. **98**, 186806 (2007).

[6] A. V. Nalitov, L. E. Golub, and E. L. Ivchenko, Ratchet effects in two-dimensional systems with a lateral periodic potential, Phys. Rev. B **86**, 115301 (2012).

[7] M. Glazov and S. Ganichev, High frequency electric field induced nonlinear effects in graphene, Phys. Rep. **535**, 101 (2014).

[8] J. Karch, C. Drexler, P. Olbrich, M. Fehrenbacher, M. Hirmer, M. M. Glazov, S. A. Tarasenko, E. L. Ivchenko, B. Birkner, J. Eroms, D. Weiss, R. Yakimova, S. Lara-Avila, S. Kubatkin, M. Ostler, T. Seyller, and S. D. Ganichev, Terahertz Radiation Driven Chiral Edge Currents in Graphene, Phys. Rev. Lett. **107**, 276601 (2011).

[9] P. Dollfus *et al.*, Thermoelectric effects in graphene nanostructures, J. Phys.: Condens. Matter **27**, 133204 (2015).

[10] A. A. Balandin, Thermal properties of graphene and nanostructured carbon materials, Nat. Mater. **10**, 569 (2011).

[11] D. L. Nika and A. A. Balandin, Two-dimensional phonon transport in graphene, J. Phys.: Condens. Matter **24**, 233203 (2012).

[12] X. Gu and R. Yang, Phonon transport and thermal conductivity in two-dimensional materials, arXiv:1509.07762v2.

[13] X. Xu, J. Chen, and B. Li, Phonon thermal conduction in novel 2D materials, J. Phys.: Condens. Matter **28**, 483001 (2016).

[14] T. Ando, Screening effect and impurity scattering in monolayer graphene, J. Phys. Soc. Jpn. **75**, 074716 (2006).

[15] M. Ishigami, J. H. Chen, W. G. Cullen, M. S. Fuhrer, and E. D. Williams, Atomic structure of graphene on SiO_2, Nano Lett. **7**, 1643 (2007).

[16] S. V. Morozov, K. S. Novoselov, M. I. Katsnelson, F. Schedin, D. C. Elias, J. A. Jaszczak, and A. K. Geim, Giant Intrinsic Carrier Mobilities in Graphene and its Bilayer, Phys. Rev. Lett. **100**, 016602 (2008).

[17] M. Katsnelson and A. Geim, Electron scattering on microscopic corrugations in graphene, Philos. Trans. R. Soc. London A **366**, 195 (2008).

[18] H. Sevinçli and M. Brandbyge, Phonon scattering in graphene over substrate steps, Appl. Phys. Lett. **105**, 153108 (2014).

[19] J.-H. Chen, C. Jang, S. Xiao, M. Ishigami, and M. S. Fuhrer, Intrinsic and extrinsic performance limits of graphene devices on SiO_2, Nat. Nano **3**, 206 (2008).

[20] S. Fratini and F. Guinea, Substrate-limited electron dynamics in graphene, Phys. Rev. B **77**, 195415 (2008).

[21] V. Perebeinos and P. Avouris, Inelastic scattering and current saturation in graphene, Phys. Rev. B **81**, 195442 (2010).

[22] S. S. Kubakaddi and K. S. Bhargavi, Enhancement of phonon-drag thermopower in bilayer graphene, Phys. Rev. B **82**, 155410 (2010).

[23] S. Koniakhin and E. Eidelman, Phonon drag thermopower in graphene in equipartition regime, Europhys. Lett. **103**, 37006 (2013).

[24] W. Cai, A. L. Moore, Y. Zhu, X. Li, S. Chen, L. Shi, and R. S. Ruoff, Thermal transport in suspended and supported monolayer graphene grown by chemical vapor deposition, Nano Lett. **10**, 1645 (2010).

[25] S. Chen *et al.*, Raman measurements of thermal transport in suspended monolayer graphene of variable sizes in vacuum and gaseous environments, ACS Nano **5**, 321 (2010).

[26] S. Ghosh, I. Calizo, D. Teweldebrhan, E. Pokatilov, D. Nika, A. Balandin, W. Bao, F. Miao, and C. N. Lau, Extremely high thermal conductivity of graphene: Prospects for thermal management applications in nanoelectronic circuits, Appl. Phys. Lett. **92**, 151911 (2008).

[27] A. A. Balandin, S. Ghosh, W. Bao, I. Calizo, D. Teweldebrhan, F. Miao, and C. N. Lau, Superior thermal conductivity of single-layer graphene, Nano Lett. **8**, 902 (2008).

[28] C. Faugeras, B. Faugeras, M. Orlita, M. Potemski, R. R. Nair, and A. Geim, Thermal conductivity of graphene in corbino membrane geometry, ACS Nano **4**, 1889 (2010).

[29] S. Chen, Q. Wu, C. Mishra, J. Kang, H. Zhang, K. Cho, W. Cai, A. A. Balandin, and R. S. Ruoff, Thermal conductivity of isotopically modified graphene, Nat. Mater. **11**, 203 (2012).

[30] J. H. Seol, I. Jo, A. L. Moore, L. Lindsay, Z. H. Aitken, M. T. Pettes, X. Li, Z. Yao, R. Huang, D. Broido *et al.*, Two-dimensional phonon transport in supported graphene, Science **328**, 213 (2010).

[31] R. Murali, Y. Yang, K. Brenner, T. Beck, and J. D. Meindl, Breakdown current density of graphene nanoribbons, Appl. Phys. Lett. **94**, 243114 (2009).

[32] A. D. Liao, J. Z. Wu, X. Wang, K. Tahy, D. Jena, H. Dai, and E. Pop, Thermally Limited Current Carrying Ability of Graphene Nanoribbons, Phys. Rev. Lett. **106**, 256801 (2011).

[33] A. Alofi and G. P. Srivastava, Phonon conductivity in graphene, J. Appl. Phys. **112**, 013517 (2012).

[34] D. L. Nika, E. P. Pokatilov, A. S. Askerov, and A. A. Balandin, Phonon thermal conduction in graphene: Role of umklapp and edge roughness scattering, Phys. Rev. B **79**, 155413 (2009).

[35] D. Nika, S. Ghosh, E. Pokatilov, and A. Balandin, Lattice thermal conductivity of graphene flakes: Comparison with bulk graphite, Appl. Phys. Lett. **94**, 203103 (2009).

[36] P. Klemens and D. Pedraza, Thermal conductivity of graphite in the basal plane, Carbon **32**, 735 (1994).

[37] P. Klemens, The scattering of low-frequency lattice waves by static imperfections, Proc. Phys. Soc. London, Sect. A **68**, 1113 (1955).

[38] H. Zhang, G. Lee, and K. Cho, Thermal transport in graphene and effects of vacancy defects, Phys. Rev. B **84**, 115460 (2011).

[39] Z. Wei, Z. Ni, K. Bi, M. Chen, and Y. Chen, In-plane lattice thermal conductivities of multilayer graphene films, Carbon **49**, 2653 (2011).

[40] T. Zhu and E. Ertekin, Phonons, localization, and thermal conductivity of diamond nanothreads and amorphous graphene, Nano Lett. **16**, 4763 (2016).

[41] T. Zhu and E. Ertekin, Phonon transport on two-dimensional graphene/boron nitride superlattices, Phys. Rev. B **90**, 195209 (2014).

[42] Z.-Y. Ong, E. Pop, and J. Shiomi, Reduction of phonon lifetimes and thermal conductivity of a carbon nanotube on amorphous silica, Phys. Rev. B **84**, 165418 (2011).

[43] D. Donadio and G. Galli, Thermal Conductivity of Isolated and Interacting Carbon Nanotubes: Comparing Results from Molecular Dynamics and the Boltzmann Transport Equation, Phys. Rev. Lett. **99**, 255502 (2007).

[44] B. Qiu and X. Ruan, Reduction of spectral phonon relaxation times from suspended to supported graphene, Appl. Phys. Lett. **100**, 193101 (2012).

[45] Z.-Y. Ong and E. Pop, Effect of substrate modes on thermal transport in supported graphene, Phys. Rev. B **84**, 075471 (2011).

[46] A. Gobel, D. T. Wang, M. Cardona, L. Pintschovius, W. Reichardt, J. Kulda, N. M. Pyka, K. Itoh, and E. E. Haller, Effects of isotope disorder on energies and lifetimes of phonons in germanium, Phys. Rev. B **58**, 10510 (1998).

[47] L. Lindsay, D. A. Broido, and N. Mingo, Flexural phonons and thermal transport in graphene, Phys. Rev. B **82**, 115427 (2010).

[48] D. Singh, J. Y. Murthy, and T. S. Fisher, Spectral Phonon Conduction and Dominant Scattering Pathways in Graphene, J. Appl. Phys. **110**, 094312 (2011).

[49] B. Amorim and F. Guinea, Flexural mode of graphene on a substrate, Phys. Rev. B **88**, 115418 (2013).

[50] B. Hess, C. Kutzner, D. van der Spoel, and E. Lindahl, Gromacs 4: Algorithms for highly efficient, load-balanced, and scalable molecular simulation, J. Chem. Theory Comp. **4**, 435 (2008).

[51] O. Dubay and G. Kresse, Accurate density functional calculations for the phonon dispersion relations of graphite layer and carbon nanotubes, Phys. Rev. B **67**, 035401 (2003).

[52] G. Bussi, D. Donadio, and M. Parrinello, Canonical sampling through velocity rescaling, J. Chem. Phys. **126**, 014101 (2007).

[53] Wolfram Research, MATHEMATICA 8.0 (2010).

[54] B. N. J. Persson and H. Ueba, Heat transfer between weakly coupled systems: Graphene on a-SiO_2, Europhys. Lett. **91**, 56001 (2010).

[55] T. Nihira and T. Iwata, Temperature dependence of lattice vibrations and analysis of the specific heat of graphite, Phys. Rev. B **68**, 134305 (2003).

[56] A. Chaudhuri, A. Kundu, D. Roy, A. Dhar, J. L. Lebowitz, and H. Spohn, Heat transport and phonon localization in mass-disordered harmonic crystals, Phys. Rev. B **81**, 064301 (2010).

[57] M. N. Luckyanova, J. Mendoza, H. Lu, S. Huang, J. Zhou, M. Li, B. J. Kirby, A. J. Grutter, A. A. Puretzky, M. S. Dresselhaus *et al.*, Phonon localization in heat conduction, arXiv:1602.05057.

[58] O. I. Utesov, A. V. Sizanov, and A. V. Syromyatnikov, Localized and propagating excitations in gapped phases of spin systems with bond disorder, Phys. Rev. B **90**, 155121 (2014).

[59] L. Chen and S. Kumar, Thermal Transport in Graphene Supported on Copper, J. Appl. Phys. **112**, 043502 (2012).

[60] G. P. Srivastava, *The Physics of Phonons* (Hilger, Bristol, 1990).

[61] J. Callaway, Model for lattice thermal conductivity at low temperatures, Phys. Rev. **113**, 1046 (1959).

[62] Z. Wei, J. Yang, K. Bi, and Y. Chen, Mode dependent lattice thermal conductivity of single layer graphene, J. Appl. Phys. **116**, 153503 (2014).

[63] J. Tersoff, Empirical Interatomic Potential for Carbon, with Applications to Amorphous Carbon, Phys. Rev. Lett. **61**, 2879 (1988).

[64] L. Lindsay and D. A. Broido, Optimized tersoff and brenner empirical potential parameters for lattice dynamics and phonon thermal transport in carbon nanotubes and graphene, Phys. Rev. B **81**, 205441 (2010).

[65] V. Geringer, M. Liebmann, T. Echtermeyer, S. Runte, M. Schmidt, R. Rückamp, M. C. Lemme, and M. Morgenstern, Intrinsic and Extrinsic Corrugation of Monolayer Graphene Deposited on SiO_2, Phys. Rev. Lett. **102**, 076102 (2009).